Role of *Toxoplasma gondii* Chloroquine Resistance Transporter in Bradyzoite Viability and Digestive Vacuole Maintenance

Geetha Kannan,[a] Manlio Di Cristina,[b] Aric J. Schultz,[a]* My-Hang Huynh,[a] Fengrong Wang,[a] Tracey L. Schultz,[a] Matteo Lunghi,[b]* Isabelle Coppens,[c] Vern B. Carruthers[a]

[a]Department of Microbiology and Immunology, University of Michigan Medical School, Ann Arbor, Michigan, USA
[b]Department of Chemistry, Biology and Biotechnology, University of Perugia, Perugia, Italy
[c]Department of Molecular Microbiology and Immunology, The Johns Hopkins University Bloomberg School of Public Health, Baltimore, Maryland, USA

ABSTRACT *Toxoplasma gondii* is a ubiquitous pathogen that can cause encephalitis, congenital defects, and ocular disease. *T. gondii* has also been implicated as a risk factor for mental illness in humans. The parasite persists in the brain as slow-growing bradyzoites contained within intracellular cysts. No treatments exist to eliminate this form of parasite. Although proteolytic degradation within the parasite lysosome-like vacuolar compartment (VAC) is critical for bradyzoite viability, whether other aspects of the VAC are important for parasite persistence remains unknown. An ortholog of *Plasmodium falciparum* chloroquine resistance transporter (CRT), TgCRT, has previously been identified in *T. gondii*. To interrogate the function of TgCRT in chronic-stage bradyzoites and its role in persistence, we knocked out TgCRT in a cystogenic strain and assessed VAC size, VAC digestion of host-derived proteins and parasite autophagosomes, and the viability of *in vitro* and *in vivo* bradyzoites. We found that whereas parasites deficient in TgCRT exhibit normal digestion within the VAC, they display a markedly distended VAC and their viability is compromised both *in vitro* and *in vivo*. Interestingly, impairing VAC proteolysis in TgCRT-deficient bradyzoites restored VAC size, consistent with a role for TgCRT as a transporter of products of digestion from the VAC. In conjunction with earlier studies, our current findings suggest a functional link between TgCRT and VAC proteolysis. This study provides further evidence of a crucial role for the VAC in bradyzoite persistence and a new potential VAC target to abate chronic *Toxoplasma* infection.

IMPORTANCE Individuals chronically infected with the intracellular parasite *Toxoplasma gondii* are at risk of experiencing reactivated disease that can result in progressive loss of vision. No effective treatments exist for chronic toxoplasmosis due in part to a poor understanding of the biology underlying chronic infection and a lack of well-validated potential targets. We show here that a *T. gondii* transporter is functionally linked to protein digestion within the parasite lysosome-like organelle and that this transporter is necessary to sustain chronic infection in culture and in experimentally infected mice. Ablating the transporter results in severe bloating of the lysosome-like organelle. Together with earlier work, this study suggests the parasite's lysosome-like organelle is vital for parasite survival, thus rendering it a potential target for diminishing infection and reducing the risk of reactivated disease.

KEYWORDS *Toxoplasma gondii*, autophagy, persistence, proteolysis, transporters

Toxoplasma gondii is an opportunistic pathogen that causes encephalitis or debilitating ocular and congenital diseases in humans (1–4). It has also been implicated as a risk factor for schizophrenia and other major mental illnesses (5–8). The parasite progresses through two major life stages during infection of its intermediate hosts: the acute stage, characterized by actively replicating tachyzoites, and the chronic stage,

featuring slow-growing bradyzoite cysts that persist in muscle and brain tissue (9). While drugs exist against acute-stage tachyzoites, currently no treatments are available to combat the chronic-stage bradyzoite cysts. The development of new interventions for limiting disease from chronic infection is hindered by a lack of well-validated potential targets and understanding of the biology of *T. gondii* bradyzoites.

One avenue toward this goal is to define the contributions of proteins associated with the parasite plant-like vacuole/vacuolar compartment (VAC). The *T. gondii* VAC is a lysosome-like organelle that contains a variety of proteases, including those of the cathepsin family (10, 11). It was previously shown that *T. gondii* cathepsin protease L (TgCPL) localizes to the lumen of the VAC, where it aids in the digestion of ingested host-derived proteins and parasite autophagosomes (11–13). Diminishing the digestive function of the VAC by either genetic ablation of TgCPL or chemical inhibition of TgCPL with morpholinurea-leucine-homophenylalanine-vinyl phenyl sulfone (LHVS) revealed an critical role for the VAC in parasite viability, particularly in the bradyzoite stage (11, 13, 14).

The *T. gondii* VAC also possesses transmembrane proteins, including an orthologue of the *Plasmodium falciparum* chloroquine resistance transporter (PfCRT) (15). *Arabidopsis thaliana* expresses a homologue of PfCRT as well, which is involved in export of glutathione from plant chloroplasts (16, 17). Similarly, PfCRT has been implicated in the transport of amino acids and peptides out of the digestive vacuole and is also important for the efflux of chloroquine from the malaria digestive vacuole to the parasite cytosol (16, 17). Recent work utilizing yeast demonstrated that *T. gondii* CRT (TgCRT) is also capable of transporting chloroquine (18). Thus, similar to PfCRT, TgCRT might also transport amino acids and small peptides out of the *T. gondii* VAC and into the parasite cytosol. Two studies have revealed that *T. gondii* RH tachyzoites deficient in TgCRT, either by inducible knockdown or complete genetic ablation, exhibit an enlarged VAC (15, 18). In addition, expansion of the VAC in TgCRT-deficient tachyzoites is diminished when parasite digestion is impaired by genetic ablation of cathepsin protease B (TgCPB) or chemical inhibition of TgCPL with LHVS (18). Thus, the distended VAC in TgCRT-deficient tachyzoites was postulated to be due to increased osmotic pressure from a buildup of digestion products that could not be transported out of the VAC (15, 18). TgCRT-deficient tachyzoites also grow more slowly *in vitro* and are compromised in their ability to cause mortality in mice during acute infection, suggesting that an inability to transport digested material out of the VAC and into the parasite cytosol has a moderate effect on *T. gondii* tachyzoites (15, 18).

However, the extent to which TgCRT functions as a transporter of digestion products in bradyzoite cysts and thereby contributes to VAC morphology or function, or whether it is necessary for parasite viability during the chronic stage of infection, is unknown. We therefore sought to define the function of TgCRT in bradyzoites and its contribution to bradyzoite survival. To study this, we created a knockout of TgCRT in a cystogenic strain and assessed VAC morphology, *in vitro* and *in vivo* viability, and VAC digestion of host- or parasite-derived material in TgCRT-deficient bradyzoites. We show that these bradyzoites exhibit a severely bloated VAC, that TgCRT appears to function downstream of protein digestion within the VAC, and that TgCRT deficiency results in loss of bradyzoite viability.

RESULTS

PΔ*crt* parasites exhibit a markedly distended VAC. To examine the role of TgCRT in bradyzoites, we knocked out TgCRT in the cystogenic type II Prugniaud Δ*ku80* strain (PΔ*crt*) and restored its expression via genetic complementation (PΔ*crt:CRT*) (Fig. S1 and S2). Consistent with TgCRT playing a role in VAC morphology, PΔ*crt* extracellular tachyzoites (Fig. 1A) and bradyzoites isolated from *in vitro* cysts (Fig. 1B) show a larger translucent vacuole associated with the VAC marker TgCPL than the parental and complement strains. The translucent vacuole was also observed within intact *in vitro* TgCRT-deficient bradyzoite cysts, as seen by phase-contrast (Fig. 1C) and electron microscopy (EM) (Fig. 1D) imaging, suggesting that VAC enlargement in bradyzoites is
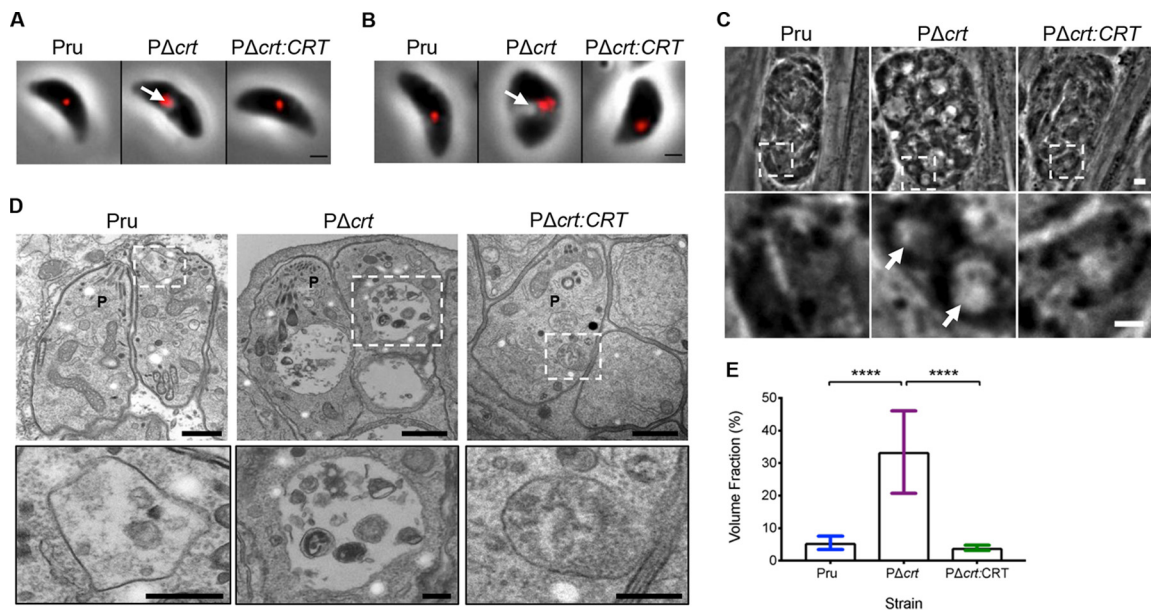
FIG 1 PΔ*crt* tachyzoites and bradyzoites exhibit a distended VAC. (A) Extracellular tachyzoites stained for the VAC protease TgCPL (red). Scale bar, 1 μm. The arrow denotes distended VAC. (B) Extracellular bradyzoites purified from *in vitro* cysts differentiated for 1 week and stained for TgCPL (red). Scale bar, 1 μm. The arrow denotes distended VAC. (C) Intracellular bradyzoite cysts differentiated *in vitro* for 1 week. Scale bar, 10 μm. The arrow denotes distended VAC. (D) Electron micrographs of intracellular bradyzoite cysts cultured *in vitro* for 1 week. Images within white boxes were expanded for the insets shown in the second row. The scale bars represent 500 nm for low-magnification images and 200 nm for the insets. P, parasite. (E) Quantification of VAC size from electron micrographs. The following numbers of VACs were measured for each strain: Pru ($n = 13$), PΔ*crt* ($n = 25$), PΔ*crt:CRT* ($n = 15$). A minimum of five images, each containing at least one cyst, was used to measure VAC size. The volume fraction corresponds to the area of the VAC/area of the parasite $\times$ 100. The bars indicate the means $\pm$ the standard deviations (SD). One-way ANOVA with Tukey's multiple comparison was performed. All genotypes were compared, and only significant differences are shown in the figure (****, $P < 0.0001$).

not strictly a consequence of being in an extracellular environment. Quantification of EM images reveals a 5-fold enlargement of VAC area in PΔ*crt* bradyzoites compared to the parental and complement strains (Fig. 1E). These results indicate that TgCRT deficiency in a cystogenic type II strain results in a pronounced enlargement of the VAC in both tachyzoites and bradyzoites.

TgCRT is required for *in vitro* bradyzoite viability and *in vivo* cyst burden. Previous work established that proteolytic digestion of material in the VAC is necessary for survival of *T. gondii* bradyzoites *in vitro* and *in vivo* (13). Because TgCRT is important for maintaining normal VAC morphology, we reasoned that TgCRT deficiency might compromise bradyzoite viability. We first wanted to address whether the lack of TgCRT affected the rate or efficiency of tachyzoite to bradyzoite conversion and bradyzoite replication. The parasite strains used express green fluorescent protein (GFP) under the early bradyzoite LDH2 promoter (19). To assess conversion, we measured the percentage of parasite-containing vacuoles with >50% coverage of GFP or the more mature-stage bradyzoite-specific marker TgBAG1 over the first 4 days of conversion. For both early- and mature-bradyzoite-stage markers analyzed, we found that all strains converted at a similar rate (Fig. S3). In addition, we measured the cyst size as an indicator of bradyzoite replication at 1 and 2 weeks postconversion and found them to be comparable among all strains at both time points (Fig. S4). These findings suggest that TgCRT is not necessary for acute to chronic-stage differentiation or replication of chronic-stage parasites up to 2 weeks *in vitro*.

We then sought to assess the extent to which TgCRT deficiency affects bradyzoite viability *in vitro*. First, we measured the expression of GFP as a proxy of bradyzoite health. It was previously shown that as bradyzoite viability decreases, there is a shift from cysts being uniformly GFP positive to partially positive (mixture of GFP positive and GFP negative) to fully GFP negative (13). Although we found that PΔ*crt* cysts were uniformly GFP positive (Fig. 2A) the intensity of GFP was diminished at 2 weeks, but not
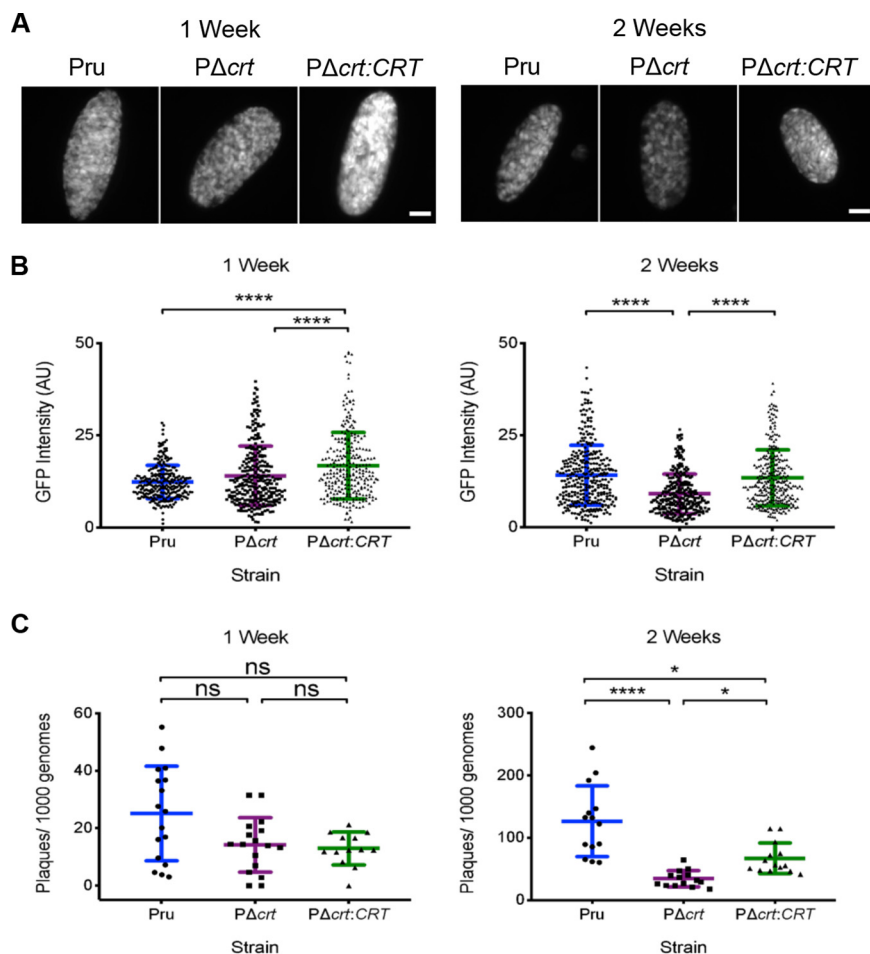
FIG 2 Deletion of CRT affects *in vitro* bradyzoite viability. (A) Fluorescent images of bradyzoite cysts expressing GFP under the early bradyzoite LDH2 promoter after 1 and 2 weeks of *in vitro* differentiation. All of the examples shown were also positive for dolichos staining. Scale bars, 10 μm. (B) GFP intensity after 1 and 2 weeks of *in vitro* differentiation. The lines represent means ± the SD of bradyzoite cysts in three independent experiments. The following numbers of cysts were analyzed for each experiment. Week 1: Pru (n = 77, 54, and 142), PΔ*crt* (n = 54, 91, and 148), PΔ*crt:CRT* (n = 96, 92, and 88). Week 2: Pru (n = 106, 124, and 102), PΔ*crt* (n = 56, 131, and 94), PΔ*crt:CRT* (n = 89, 107, and 102). The Kruskal-Wallis test with Dunn's multiple comparison was performed. GFP intensity measurements were performed on dolichos-positive cysts. All genotypes were compared, and only significant differences are shown in the figure (****, $P < 0.0001$). (C) Viability of bradyzoites after 1 and 2 weeks of *in vitro* differentiation based on plaque numbers normalized to qPCR quantification. The lines represent means ± the SD of three to four technical replicates in four to five independent experiments. The following numbers of technical replicates were analyzed for each experiment. Week 1: Pru (n = 3, 3, 3, 4, and 4); PruΔ*crt* (n = 3, 3, 3, 4, and 4); PruΔ*crt:CRT* (n = 3, 3, 3, and 4). Week 2: Pru (n = 3, 3, 3, 4, and 4); PruΔ*crt* (n = 3, 3, 3, 4, and 4); PruΔ*crt:CRT* (n = 3, 3, 3, 4, and 4). The Kruskal-Wallis test with Dunn's multiple comparison was performed (****, $P < 0.0001$; *, $P < 0.05$).

1 week, postconversion (Fig. 2B), suggesting a temporal decrease in gene expression. Next we more directly evaluated bradyzoite viability using a qPCR/plaque assay (13), which measures the ability of bradyzoites to initiate plaque formation relative to the inoculum (plaques/1000 genomes). We found that PΔ*crt* bradyzoite viability was decreased at 2 weeks, but not at 1 week, postconversion (Fig. 2C), mirroring the findings for GFP intensity. Since a decrease in plaques/genomes could be attributed to a deficiency in the ability of PΔ*crt* parasites to form plaques, we conducted a tachyzoite plaque assay that revealed PΔ*crt* tachyzoites have no deficit in the number of plaques formed (Fig. S5). Together, these findings indicate a progressive loss of PΔ*crt* bradyzoite viability *in vitro*.

To determine whether deletion of TgCRT affects the chronic infection *in vivo*, we infected C57BL/6 mice and enumerated brain cysts at 4 weeks postinfection. Mice

inoculated with PΔ*crt* tachyzoites showed an ~10-fold decrease in brain cyst burden compared to those inoculated with the parental or complement strains (Fig. 3A). The reduction in cyst burden was not due to a lack of infection since all mice were seropositive for *T. gondii* IgG, including those in which no cysts were observed (Fig. 3B). However, it is possible that the reduced number of PΔ*crt* brain cysts observed was due to fewer tachyzoites entering the brain during acute infection. To examine this, we used quantitative PCR (qPCR) to measure initial levels of infection in the brain at days 7 and 10 postinfection. Compared to those infected with parental or complement strains, mice infected with PΔ*crt* parasites showed a 2- to 3-fold-lower brain burden, suggesting that the decrease in cyst burden at 4 weeks postinfection is partly attributable to lower initial infection of the brain.

Because we found that *in vitro* TgCRT-deficient bradyzoites are less viable, we wanted to examine whether residual *in vivo* PΔ*crt* cysts are infectious. To test this, we inoculated naive mice with 5 or 30 cysts from the brains of mice chronically infected with Pru, PΔ*crt*, or PΔ*crt:CRT*. Once in the chronic phase, infection of naive mice was monitored via serology and by determining whether parasites could be cultured from their brain homogenates. To serve as a negative control, five naive mice were inoculated with brain homogenate from an uninfected mouse. All mice inoculated with PΔ*crt* brain cysts were seropositive, indicating that PΔ*crt* cysts contain infectious bradyzoites (Fig. 3D). However, only 50% of the seropositive mice were culture positive. In contrast, while not all mice inoculated with parental or complement brain cysts were seropositive, parasites were cultured from the brains of 100% of the seropositive mice. Taken together, our *in vitro* and *in vivo* data indicate that TgCRT-deficient bradyzoites show a decrease, but not an absolute loss, of viability.

Digestion in the VAC of TgCRT-deficient tachyzoites and bradyzoites. We next wanted to interrogate whether the decreased viability in TgCRT-deficient bradyzoites is possibly due to an impairment of proteolytic digestion in the VAC. Pru strain tachyzoites and bradyzoites deficient in the VAC protease TgCPL (PΔ*cpl*) have a deficit in digestion and reduced bradyzoite viability (13). It was recently suggested that RHΔ*crt* tachyzoites have 25% less TgCPL, but the extent to which this affects VAC digestion was not assessed (18). To probe whether TgCRT deficiency affects VAC digestion in tachyzoites, we utilized a tachyzoite ingestion/digestion assay that permits the detection of ingested and undigested host-derived mCherry within tachyzoites (12). We included PΔ*cpl* as a reference control since these parasites accumulate host-derived mCherry due to a deficiency in VAC proteolytic activity (11, 13, 14). We also created a PΔ*crt*Δ*cpl* double-knockout strain by ablating TgCRT in the PΔ*cpl* strain to determine whether a lack of accumulated host-derived material in PΔ*crt* parasites is due to functional digestion or problems in protein delivery to the VAC (see Fig. S1 in the supplemental material). Western blotting confirmed that TgCPL was expressed in all strains except for the PΔ*cpl* and PΔ*crt*Δ*cpl* strains (Fig. 4A). Accumulation of host-derived mCherry was observed in tachyzoites of all strains (Fig. 4B). However, we found that whereas 33% of PΔ*cpl* and 38% PΔ*crt*Δ*cpl* tachyzoites accumulated host-derived mCherry, the PΔ*crt* strain showed only 3% mCherry positive tachyzoites, which is comparable to the parental and complement lines (Fig. 4C). Accumulation of mCherry in PΔ*crt*Δ*cpl* parasites was not significantly different than that of the PΔ*cpl* strain. Taken together, these findings suggest that TgCRT is not required for the delivery or digestion of host-derived protein in the VAC of tachyzoites.

We next wanted to determine whether TgCRT deficiency affects VAC digestion in bradyzoites. Since it has not yet been shown whether bradyzoites are capable of ingesting host cytosolic material akin to tachyzoites, we instead employed a "puncta" assay to initially assess VAC digestion in bradyzoites. This assay is based on a previous report showing that disruption of VAC proteolysis with the TgCPL inhibitor LHVS leads to the accumulation of undigested material in the VAC, which is visible by phase-contrast microscopy as dark puncta (13). We found that PΔ*crt* cysts treated with LHVS developed dark puncta and that this corresponded with loss of the translucent VAC
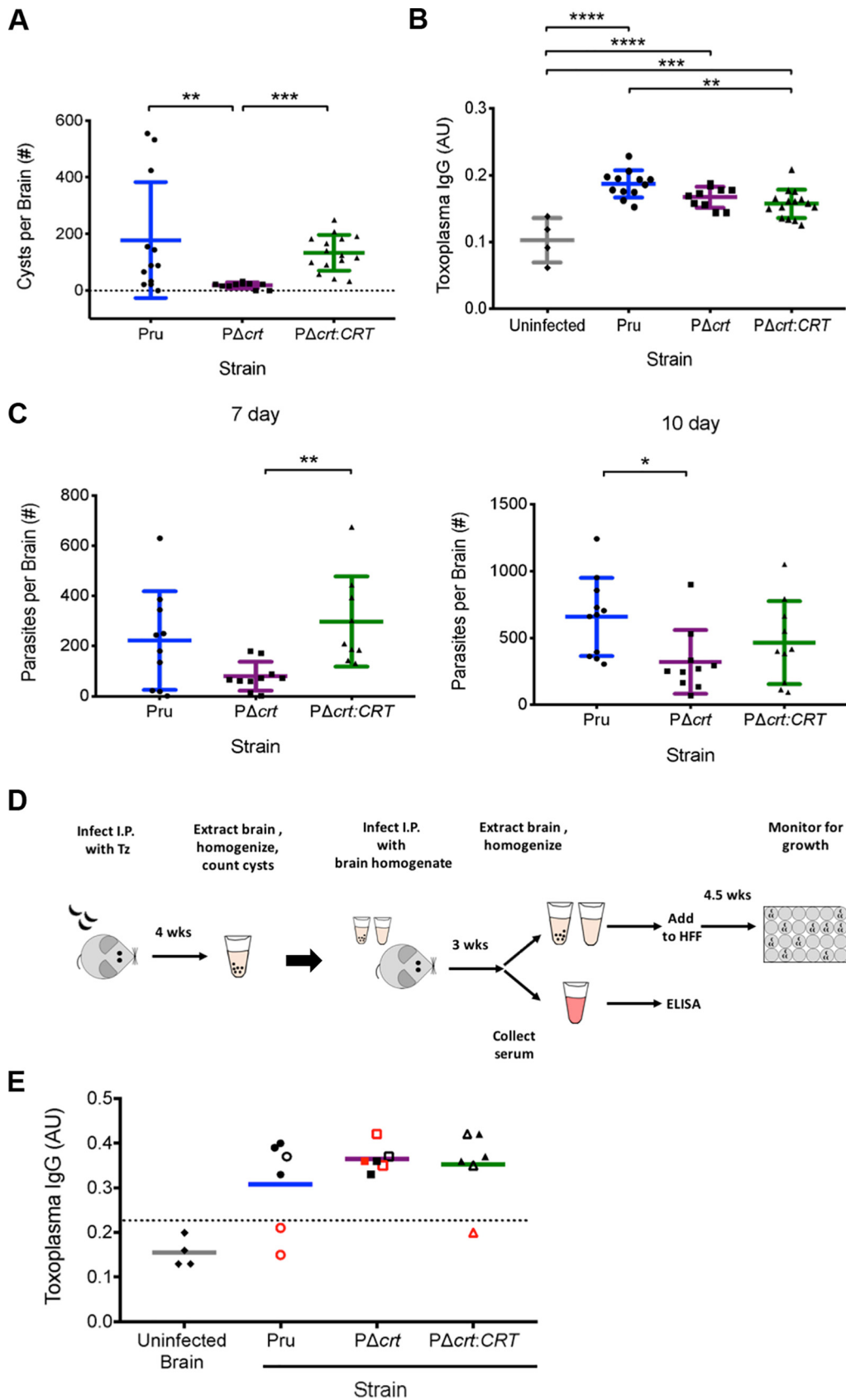
FIG 3 Deletion of TgCRT affects *in vivo* bradyzoite burden. (A) Brain cyst burdens in mice at 4 weeks postinfection with *T. gondii*. Lines represent the means ± the SD of mice from two independent experiments. The total numbers of mice
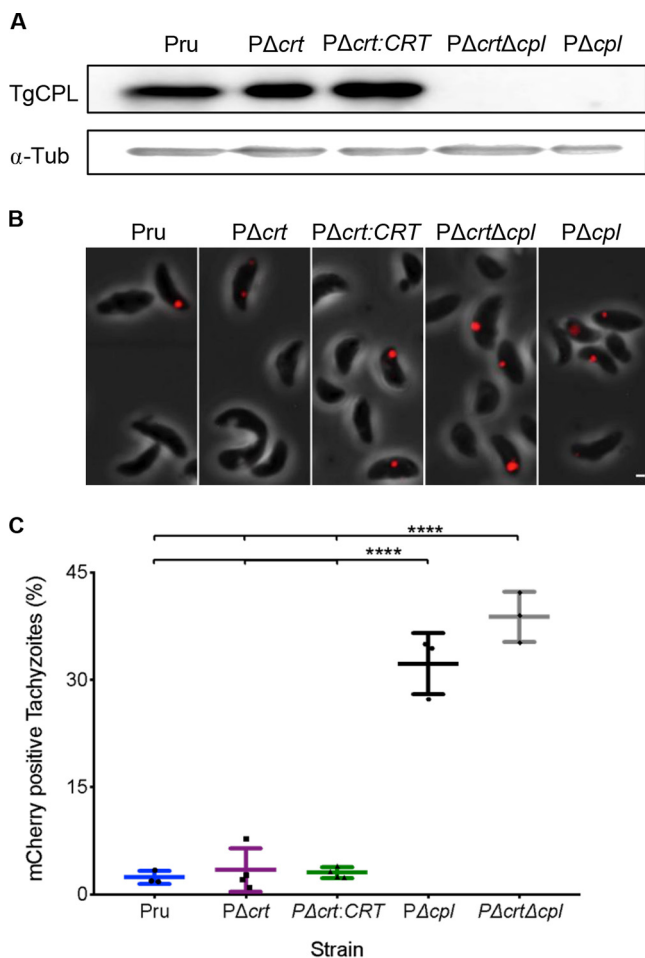
(Continued on next page)

FIG 4 VAC digestive function is not altered in PΔ*crt* tachyzoites. (A) Western blot of tachyzoite lysates probed for TgCPL (~30 kDa) and α-tubulin (~55 kDa) as a loading control. (B) Representative images of tachyzoites with ingested host-derived mCherry in red. Scale bar, 1 μm. (C) Tachyzoite ingestion/digestion assay quantification from panel B. Lines represent the means ± the SD of three to four experiments. The following numbers of tachyzoites were enumerated for each experiment: Pru (n = 234, 370, and 280), PΔ*crt* (n = 297, 258, 290, and 241), PΔ*crt:CRT* (n = 235, 282, 239, and 466), PΔ*crt*Δ*cpl* (n = 268, 211, and 270), and PΔ*cpl* (n = 426, 384, and 275). All genotypes were compared, and only significant differences are shown in the figure. One-way ANOVA with Holm-Sidak's multiple comparisons was performed (****, $P < 0.0001$).

(Fig. 5A and B). As expected, there was an increase in dark puncta of parental and complement LHVS-treated cysts as well. However, PΔ*crt* cysts contain larger dark puncta in both dimethyl sulfoxide (DMSO)- and LHVS-treated samples than in the parental and complement cysts (Fig. 5B). Also, although PΔ*crt* bradyzoites did not show

FIG 3 Legend (Continued)
analyzed were as follows: Pru (n = 12), PΔ*crt* (n = 10), and PΔ*crt:CRT* (n = 15). The Kruskal-Wallis test with Dunn's multiple comparison was performed. All genotypes were compared, and only significant differences are shown in the figure (***, P = 0.0002; **, P = 0.0098). (B) *T. gondii* IgG in mice infected in panel A. Age- and sex-matched uninfected mice were used as an IgG- negative control. One-way ANOVA with Holm-Sidak's multiple comparisons was performed. All groups were compared, and only significant differences are shown in the figure (****, $P < 0.0001$; ***, P = 0.0002; **, P = 0.002). (C) Brain parasite burdens at 7 and 10 days postinfection. The lines indicate the means ± the SD of mice from two independent experiments. The Kruskal-Wallis test with Dunn's multiple comparisons was performed. The following numbers of mice were analyzed for 7 and 10 days postinfection, respectively: Pru (n = 10 and 11), PΔ*crt* (n = 10 and 10), and PΔ*crt:CRT* (n = 9 and 10). All genotypes were compared, and only significant differences are shown in the figure (**, P = 0.005; *, P = 0.017). (D) Diagram of the experiments performed for generating the data in panel E. More detailed information can be found in Materials and Methods. (E) *T. gondii* IgG levels in mice administered residual brain cysts (5 or 30 cysts). The data are from one experiment. The line shows the mean, and the dotted line is 2 SD above the mean of mice given uninfected brain homogenate. Open symbols denote mice administered 5 parasite cysts, and closed symbols denote mice administered 30 parasite cysts. Red symbols denote no parasite growth from brain homogenate. Total numbers of mice analyzed: uninfected mice (n = 4), Pru (n = 6), PΔ*crt* (n = 6), and PΔ*crt:CRT* (n = 6).
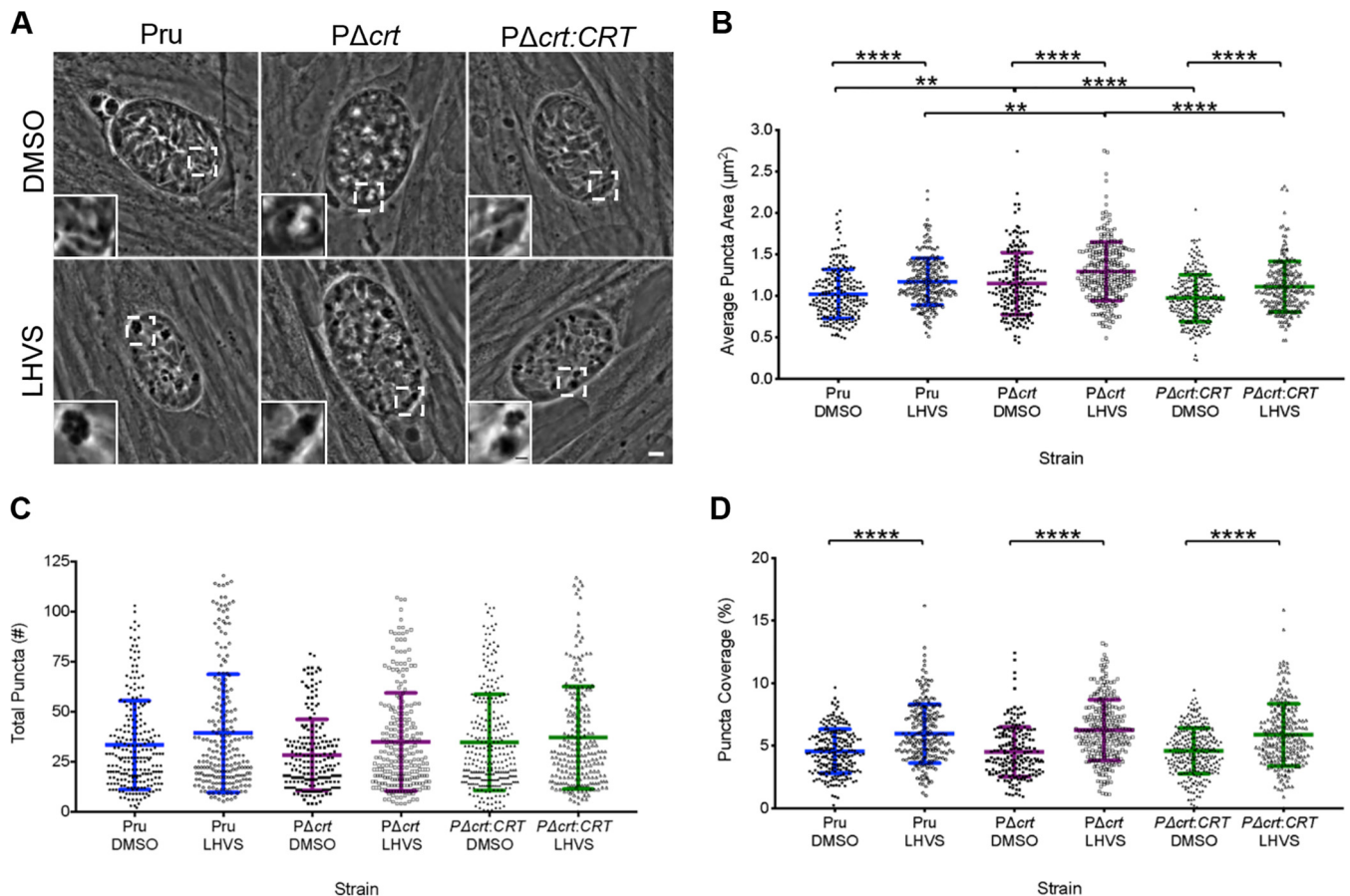
FIG 5 VAC digestive function is not altered in PΔcrt bradyzoites. (A) Representative images of bradyzoite cysts cultured in vitro for 7 days and then treated with DMSO as a vehicle control or 1 μM LHVS for 3 days. Dark puncta are clearly seen in LHVS-treated cysts. The scale bar represents 5 μm, and the scale bar in the inset represents 1 μm. (B) Measurement of dark puncta area within cysts from three independent experiments. Lines represent means ± the SD. The following numbers of cysts were analyzed from each experiment: Pru DMSO (n = 66, 69, and 102), Pru LHVS (n = 69, 74, and 87), PΔcrt DMSO (n = 72, 59, and 69), PΔcrt LHVS (n = 109, 78, and 70), PΔcrt:CRT DMSO (n = 115, 60, and 105), PΔcrt:CRT LHVS (n = 77, 56, and 94). The Kruskal-Wallis test with Dunn's multiple comparisons was performed. All treatment groups within each genotype and all genotypes within each treatment group were compared, and only significant differences are shown in the figure (****, P < 0.0001; **, P < 0.01). (C) Total puncta number in cysts analyzed in panel B. Lines represent means ± the SD. The following numbers of cysts were analyzed from each experiment: Pru DMSO (n = 64, 68, and 99), Pru LHVS (n = 65, 71, and 86), PΔcrt DMSO (n = 70, 58, and 66), PΔcrt LHVS (n = 107, 74, and 65), PΔcrt:CRT DMSO (n = 112, 58, and 106), and PΔcrt:CRT LHVS (n = 73, 56, and 87). A Kruskal-Wallis test with Dunn's multiple comparison was performed. All treatment groups within each genotype and all genotypes within each treatment group were compared, and only significant differences are shown in the figure. (D) Percent puncta coverage for each cyst analyzed in panel B. Lines represent means ± the SD. The following numbers of cysts were analyzed from each experiment: Pru DMSO (n = 66, 69, and 103), Pru LHVS (n = 69, 74, and 87), PΔcrt DMSO (n = 72, 59, and 69), PΔcrt LHVS (n = 109, 78, and 70), PΔcrt:CRT DMSO (n = 113, 60, and 106), and PΔcrt:CRT LHVS (n = 77, 56, and 94). A Kruskal-Wallis test with Dunn's multiple comparison was performed. All treatment groups within each genotype and all genotypes within each treatment group were compared, and only significant differences are shown in the figure (****, P < 0.0001).

an increase in the total number of puncta (Fig. 5C), the percentage of total cyst area occupied by puncta was increased with LHVS treatment (Fig. 5D). Together, these findings suggest that PΔcrt bradyzoites have larger puncta as an indicator of undigested material; however, whether this is a result of moderately impaired proteolytic digestion within the VAC or the intrinsically larger size of PΔcrt VAC is unclear.

The dark puncta observed within LHVS-treated bradyzoite cysts have been shown to colocalize with TgCPL and T. gondii autophagy-related protein 8 (TgAtg8), suggesting that some of the undigested material found within the bradyzoite VAC is derived from autophagy (13). To interrogate whether TgCRT deficiency affects the production or turnover of parasite autophagosomes, we created a PΔcrt strain that ectopically expresses tdTomato-TgAtg8 (Fig. S2), as done previously for Pru (13). Abundance of tdTomato-TgAtg8 in DMSO-treated bradyzoites is a function of autophagosomal production and turnover. In contrast, tdTomato-TgAtg8 abundance in LHVS-treated bradyzoites is a function of autophagosomal production exclusively since turnover is

blocked. Pru and PΔ*crt* tdTomato-TgAtg8 cysts treated with DMSO or LHVS for 1 or 3 days were assessed for tdTomato-TgAtg8 intensity both within cysts and in isolated bradyzoites. We also measured the total area of tdTomato-TgAtg8 puncta within cysts. For the DMSO control, no significant differences were seen between Pru and PΔ*crt* parasites for tdTomato-TgAtg8 intensity in intact cysts (Fig. 6A and B) or isolated bradyzoites (Fig. 6C), suggesting no change in the balance of autophagosome production and turnover. DMSO-treated PΔ*crt* bradyzoites showed a modest, but significant, increase in tdTomato-TgAtg8 puncta size (Fig. 6D), potentially due to tdTomato-TgAtg8 association with the enlarged VAC in such parasites. Upon inhibition of VAC proteolysis with LHVS, tdTomato-TgAtg8 intensity and size increased progressively for both Pru and PΔ*crt* bradyzoites. However, accumulation of tdTomato-TgAtg8 in PΔ*crt* bradyzoites was delayed and somewhat muted compared to Pru. Taken together, these data suggest that the balance of autophagosome production and turnover is unchanged in PΔ*crt* but that TgCRT deficiency is associated an overall lower rate of autophagosome production.

TgCRT transport function is linked to VAC proteolysis. Malaria parasites bearing chloroquine resistance mutations in PfCRT display an enlarged digestive vacuole, and they accumulate small peptides derived from hemoglobin (20, 21). This, combined with other work showing that recombinant PfCRT transports amino acids, small peptides, and chloroquine (17), suggests that PfCRT functions to transport products of hemoglobin digestion out of the digestive vacuole. More recently, TgCRT was also shown to transport chloroquine upon heterologous expression in yeast, providing evidence that it functions as a transporter (18). It is therefore plausible that TgCRT is also able to transport amino acids and small peptides out of the VAC. If TgCRT plays a similar role and the swelling of the VAC in PΔ*crt* parasites is due to a buildup of TgCRT substrates derived from protein digestion, then reducing the production of digestion products by inhibiting TgCPL should prevent or reverse VAC enlargement.

To test this, we differentiated PΔ*crt* bradyzoites 7 days before adding LHVS for another 2 days under differentiation conditions. This treatment window was chosen because our earlier results showed that 3 days of LHVS treatment results in larger dark and Atg8 puncta areas (Fig. 5B and 6D), whereas a 1-day treatment appeared to have no notable effect on Atg8 intensity (Fig. 5B and C). We reasoned that with 2 days of treatment, we should begin seeing an effect of LHVS treatment on VAC size prior to excessive accumulation of undigested protein. Although some enlarged VACs were apparent in LHVS treated PΔ*crt* bradyzoites (Fig. 7A), quantification revealed a significant restoration of VAC size upon LHVS treatment (Fig. 7B). Also, undigested material accumulated within the VAC of PΔ*crt* bradyzoites treated with LHVS, suggesting that TgCPL is active in PΔ*crt* bradyzoites.

To validate a link between TgCRT transport function and VAC proteolysis, we compared the size and appearance of the VAC in PΔ*crt* bradyzoites with that of Pru or PΔ*crt*Δ*cpl* parasites. We found that after 4 or 7 days of conversion to bradyzoite cysts, PΔ*crt*Δ*cpl* bradyzoites have visually smaller VACs full of electron-dense, undigested material compared to the markedly enlarged, more electron-lucent VACs of PΔ*crt* bradyzoites (Fig. 7C). Quantification revealed VAC size of PΔ*crt*Δ*cpl* strains to be significantly smaller than PΔ*crt* VACs at both time points (Fig. 7D). These findings indicate that by genetically limiting proteolysis in the VAC, the gross enlargement of the VAC observed in PΔ*crt* bradyzoites is prevented. In addition, whereas approximately 15% of PΔ*crt* cysts were dead or dying at both 4 and 7 days postconversion (18/115 cysts and 11/76 cysts, respectively), 40% (26/65 cysts) of the PΔ*crt*Δ*cpl* cysts were degenerate at 4 days, and 91.3% (21/23) were degenerate at 7 days postconversion. Thus, parasites lacking both TgCRT and TgCPL appear to be more severely compromised than those lacking TgCRT alone. Taken together, our findings suggest a link between TgCRT and protein digestion in a manner that is consistent with TgCRT acting as an exporter of degradation products generated by VAC proteases in bradyzoites.
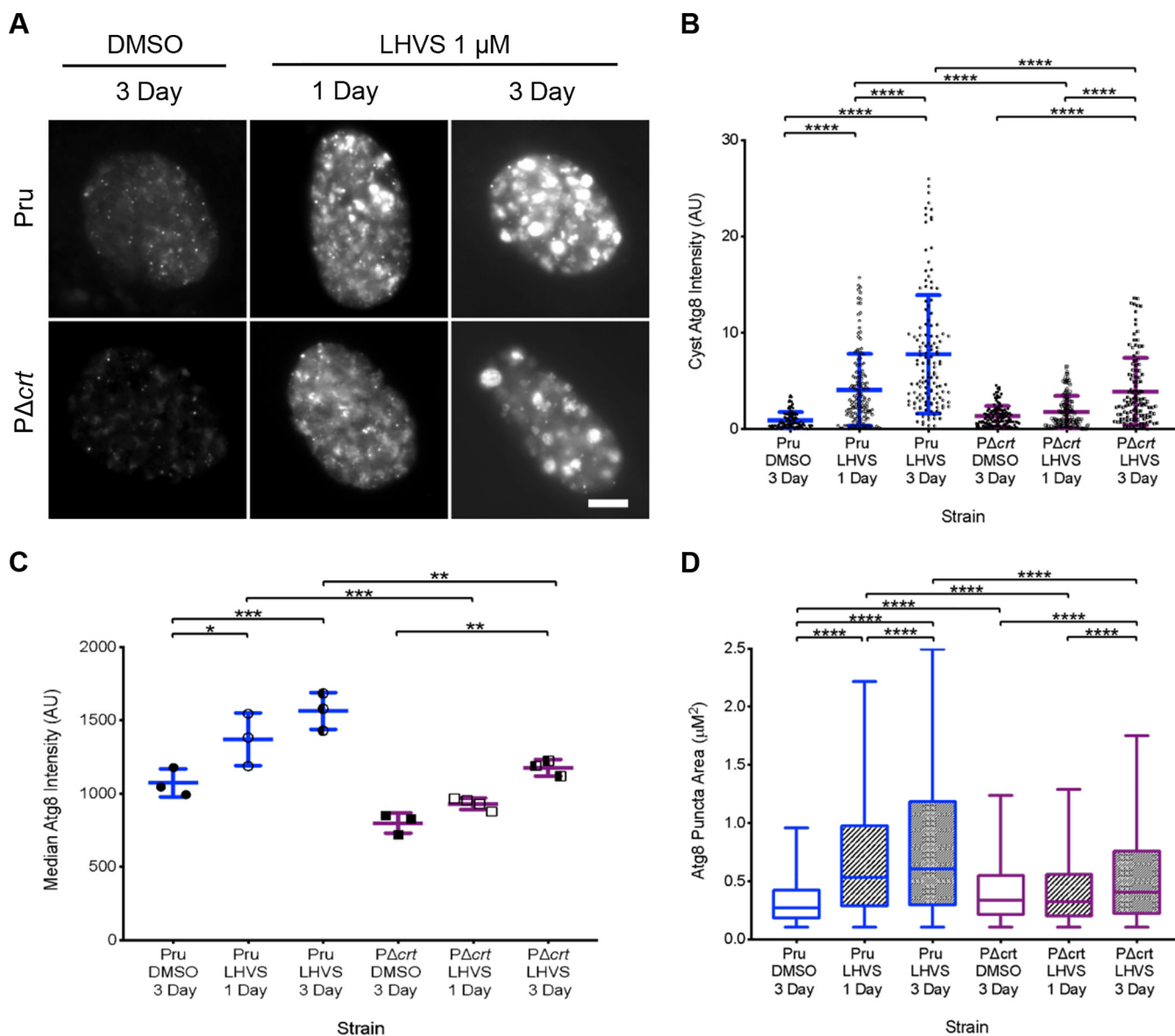
FIG 6 Autophagy in PΔ*crt* bradyzoites. (A) Representative images of Pru and PΔ*crt* Atg8-tdTomato-expressing strains after 7 days of conversion and treatment with DMSO or 1 μM LHVS for 1 or 3 days. All of the examples shown were also positive for dolichos staining. Scale bar, 10 μm. (B) Total tdTomato-TgAtg8 intensity within parasite cysts converted and treated as in panel A. The line represents the means ± the SD from three to four independent experiments. Measurements were performed on dolichos-positive cysts. The following number of cysts were analyzed in each experiment: Pru DMSO (*n* = 46, 50, and 26), Pru LHVS 1 day (*n* = 43, 47, 47, and 16), Pru LHVS 3 day (*n* = 45, 60, and 31), PΔ*crt* DMSO (*n* = 48, 54, and 30), PΔ*crt* LHVS 1 day (*n* = 37, 39, 58, and 28), and PΔ*crt* LHVS 3 day (*n* = 59, 47, and 16). A Kruskal-Wallis test with Dunn's multiple comparison was performed. All treatment groups within each genotype and all genotypes within each treatment group were compared, and only significant differences are shown in the figure (****, *P* < 0.0001; **, *P* < 0.01). (C) Atg8 intensity of bradyzoites analyzed by flow cytometry. The lines represent means ± the SD from three to four independent experiments. Measurements were performed on dolichos-positive cysts. The following numbers of bradyzoites that were GFP and TdTomato positive were analyzed in each experiment: Pru DMSO (*n* = 1,122, 5,330, and 1,534), Pru LHVS 1 day (*n* = 493, 3,199, and 613), Pru LHVS 3 day (*n* = 1,960, 5,205, and 2,043), PΔ*crt* DMSO (*n* = 620, 1,115, and 139), PΔ*crt* LHVS 1 day (*n* = 623, 962, 230, and 1,355), and PΔ*crt* LHVS 3 day (1,802, 2,641, and 337). One-way ANOVA with Sidak's multiple comparison was performed. All treatment groups within each genotype and all genotypes within each treatment group were compared, and only significant differences are shown in the figure (***,s *P* < 0.001; **, *P* < 0.01; *, *P* < 0.05). (D) tdTomato-TgAtg8 puncta size was measured for every puncta in each cyst. The lines represent means ± the SD from three to four independent experiments. Measurements were performed on dolichos-positive cysts. The following number of puncta were analyzed in each experiment: Pru DMSO (*n* = 364, 290, and 242), Pru LHVS 1 day (*n* = 617, 301, 1,826, and 1,147), Pru LHVS 3 day (*n* = 722, 697, 1,518, and 36), PΔ*crt* DMSO (*n* = 406, 427, and 330), PΔ*crt* LHVS 1 day (*n* = 277, 233, 484, and 324), and PΔ*crt* LHVS 3 day (*n* = 692, 402, and 633). A Kruskal-Wallis test with Dunn's multiple comparison was performed. All treatment groups within each genotype and all genotypes within each treatment group were compared, and only significant differences are shown in the figure (****, *P* < 0.0001).

DISCUSSION

We show here that TgCRT is necessary for maintaining the size of the VAC and the viability of *T. gondii* bradyzoites, possibly by functioning as a transporter of digested material from the VAC to the parasite cytosol. Together with other recent studies
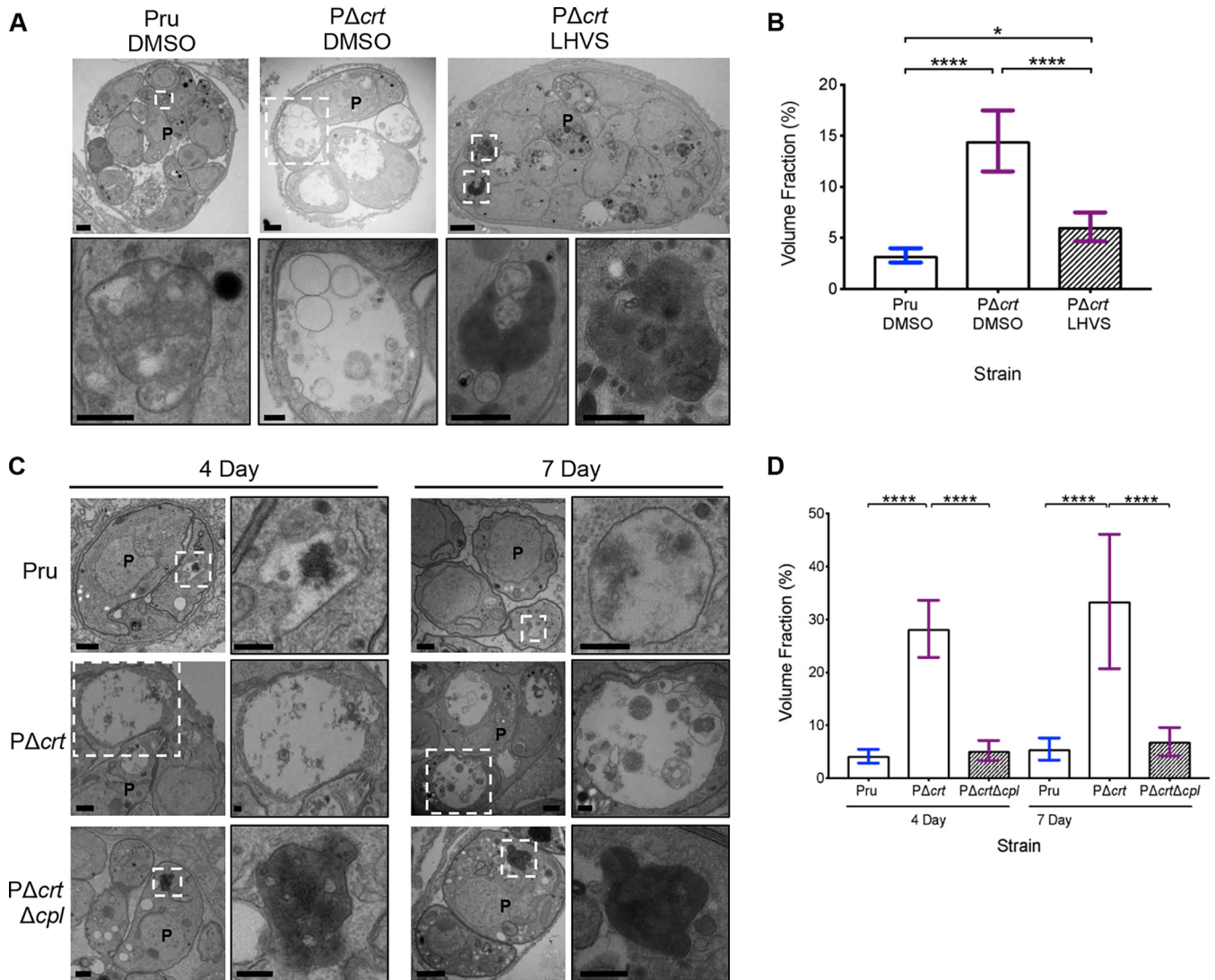
FIG 7 VAC digestion disruption through CPL modulation affects PΔ*crt* bradyzoite VAC size and parasite health. (A) Electron microscopy of *in vitro* bradyzoite cysts converted for 7 days and then treated with DMSO and 1 μM LHVS for 2 days. Scale bars, 500 nm. (B) Quantification of VACs in panel A. Bars represent means ± the SD. The following numbers of VACs were measured for each strain: Pru (n = 18), PΔ*crt* DMSO (n = 49), and PΔ*crt* LHVS (n = 13). One-way ANOVA testing with Tukey's multiple comparison was performed. All treatment groups within each genotype and all genotypes within each treatment group were compared, and only significant differences are shown in the figure (****, $P < 0.0001$; *, $P < 0.05$). (C) Representative electron micrograph images of *in vitro* bradyzoite cysts converted for 4 day and 7 days. Scale bars, 500 nm. P, parasite. (D) Quantification of VACs in panel C. Bars represent means ± the SD. The following numbers of VACs were measured for each strain: 4-day Pru (n = 16), PΔ*crt* (n = 17), and PΔ*crt*Δ*cpl* (n = 17) and 7-day Pru (n = 13), PΔ*crt* (n = 25), and PΔ*crt*Δ*cpl* (n = 35). One-way ANOVA with Tukey's multiple comparison was performed. All genotypes for each time point were compared, and only significant differences are shown (****, $P < 0.0001$). The 7-day Pru and PΔ*crt* data were also used in Fig. 1.

reporting that VAC protein digestion is crucial for bradyzoite viability (13), our findings point toward the VAC as an important organelle for *T. gondii* bradyzoite persistence and uncover TgCRT as a potential target for chronic *T. gondii* infection.

Our finding that deletion of TgCRT in a type II strain (PΔ*crt*) resulted in enlargement of the VAC is in line with previous studies that have knocked down (15) or knocked out (18) TgCRT in a type I strain (RH). We also show that this enlarged VAC phenotype is consistent across life stages and that it appears to be especially prominent in bradyzoites. Our EM measurements suggest that the VAC occupies one-third of the cytoplasm of PΔ*crt* bradyzoites, thus becoming easily visible by phase-contrast microscopy in many parasites. VAC enlargement was fully reversed upon reexpression of TgCRT, firmly establishing that TgCRT expression is necessary to maintain normal VAC morphology.

The underlying basis for enlargement of the VAC in TgCRT-deficient parasites is unknown, but it may be linked to endolysosomal system dynamics and the transporter function of TgCRT. The VAC is a dynamic organelle that undergoes rounds of fission to form smaller structures late in the cell cycle before fusing to form typically a single compartment in G_1 phase (10, 22). The VAC probably also communicates via fusion and fission with the parasite endosome-like compartments (ELCs), based on partial colocalization of VAC and ELC markers in intracellular parasites (10, 18, 22). Interestingly, it was recently reported that replicating PΔ*crt* parasites maintain a single VAC that overlaps substantially with ELC markers (18). These findings imply that defects in VAC fragmentation and fission of the VAC from the ELCs result in sustaining a hybrid VAC/ELC compartment in parasites lacking TgCRT. Thus, contributions of membrane from both the VAC and ELCs could account for enlargement of the VAC in PΔ*crt* parasites. Although it is possible that TgCRT directly participates in vesicular fission, no evidence of this currently exists. On the other hand, it appears more likely that swelling of the VAC in TgCRT-deficient parasites is related to TgCRT transport function. If, akin to PfCRT, TgCRT exports proteolytic digestion products from the VAC, accumulation of such products in the VAC of PΔ*crt* parasites could increase osmotic pressure within the organelle due to the influx of water through a VAC-localized aquaporin (22). Whether a build-up of osmotic pressure is a driver of VAC size in TgCRT-deficient parasites and is thereby responsible for defective VAC fragmentation and VAC/ELC resolution awaits further study.

A knockout of *Plasmodium* CRT has not been reported, presumably because of it having an essential function. Nevertheless, chloroquine-resistant strains bearing mutations in PfCRT also exhibit an enlarged digestive vacuole. Studies with recombinant PfCRT suggested that chloroquine-resistant alleles tend to have lower transport activity for a model substrate (tetraethyl ammonium) but higher transport activity for chloroquine (17). Chloroquine-resistant strains also accumulate small peptides derived from digestion of hemoglobin (20, 21). Thus, the enlarged digestive vacuole of chloroquine-resistant strains is potentially due to a partial loss of PfCRT native transport function. That PfCRT is essential, whereas TgCRT is dispensable, likely reflects the crucial role of the malaria digestive vacuole in detoxification of heme liberated from hemoglobin digestion during replication within erythrocytes.

Consistent with an important role for TgCRT in chronic infection, we observed an ~5-fold loss of viability for PΔ*crt* bradyzoites *in vitro*. Loss of viability appears to increase with time of differentiation, suggesting a progressively important role for TgCRT in chronic infection. We also noted a 10-fold decrease in PΔ*crt* brain cysts in mice. This decrease is likely a composite of effects occurring during the acute stage and the chronic stage, which may be teased apart further via complementation of PΔ*crt* parasites with CRT expressed under stage-specific tachyzoite or bradyzoite promoters (13). The trend toward lower initial infection of the brain observed for PΔ*crt* parasites is in agreement with the decreased virulence reported during acute infection of RHΔ*crt* parasites (18). However, the lower initial infection of the brain does not appear to fully account for the striking decrease in PΔ*crt* brain cysts. Additional loss of PΔ*crt* cysts during the chronic infection of mice is consistent with our *in vitro* viability findings. Nevertheless, we found that cysts recovered from the brains of PΔ*crt* parasite-infected mice contained infectious bradyzoites capable of establishing infection of naive mice. Our observation of lower PΔ*crt* cultivation efficiency from the brains of infected naive mice is further evidence of a decreased brain burden and/or viability. Thus, whereas TgCRT is not absolutely required for *T. gondii* persistence, it nonetheless strongly influences the course and burden of chronic infection.

Proteolysis within the VAC is necessary for sustaining bradyzoite viability *in vitro* and *in vivo* (13). Genetically or chemically disrupting TgCPL activity results in a loss of bradyzoite viability that is associated with accumulation of undigested material colocalizing with Atg8, a marker of autophagosomes. *P. falciparum* parasites administered protease inhibitors that target digestive vacuole proteinases also accumulate undigested material, in this case hemoglobin derived from the infected erythrocyte (20).

However, the electron-lucent VACs observed in PΔ*crt* parasites, along with the tachyzoite ingestion assay, dark puncta measurements, and Atg8 accumulation data, suggest that digestion in PΔ*crt* tachyzoites and bradyzoites is largely normal despite the striking morphological changes to the organelle. It was suggested that RHΔ*crt* tachyzoites reduce the expression of several VAC proteases to decrease production of TgCRT substrates generated by VAC proteolysis, thereby easing osmotic pressure (18). If VAC proteolysis is similarly reduced in PΔ*crt* parasites, this does not appear to affect the digestion of host-derived protein in tachyzoites via the ingestion pathway or parasite-derived material delivered through autophagy.

Consistent with TgCRT functioning as a transporter downstream of VAC proteolysis, we found that treating PΔ*crt* bradyzoites with LHVS restored VAC size prior to subsequent accumulation of undigested material. This was observed in the EM images with 2 days of LHVS treatment, where VACs are smaller and a buildup of undigested material is beginning to show. We also found that PΔ*crt*Δ*cpl* double-knockout bradyzoites have a normal-sized VAC, confirming that protein digestion in the VAC is required for expansion of the VAC in TgCRT-deficient parasites. However, selectivity of amino acids or peptides exported out of the VAC by TgCRT within tachyzoites and bradyzoites still needs to be elucidated. The accumulation of undigested material in LHVS-treated PΔ*crt* and PΔ*crt*Δ*cpl* bradyzoites is consistent with the delivery of proteolytic substrates to the VAC TgCRT-deficient bradyzoites. Nevertheless, we noted a delay in the accumulation of the autophagic marker TgAtg8 in PΔ*crt* bradyzoites after blocking TgCPL activity with LHVS, suggesting a decrease in the production of autophagosomes. Whether this is a result of a feedback loop to reduce delivery of substrates to the VAC akin to the downregulation of proteases in TgCRT-deficient tachyzoites (18) or a due to a general decline in the health of PΔ*crt* bradyzoites remains unclear. It should also be noted that although we were unable to introduce tdTomato-TgAtg8 into PΔ*crt:crt* parasites due to a lack of available selectable markers, all of the other phenotypes measured in PΔ*crt* parasites were restored upon genetic complementation.

Previous work in TgCPL, together with the current findings for TgCRT, is consistent with a central role for the VAC in *T. gondii* persistence. Parasites deficient in TgCPL and TgCRT appear to be especially compromised, which is consistent with a functional link between these VAC components. Additional studies aimed at targeting these proteins and identifying new components of the VAC are needed to realize the potential of compromising this organelle for therapeutic gain.

MATERIALS AND METHODS

Host cell and parasite cultures. Human foreskin fibroblasts (HFFs) were grown in Dulbecco modified Eagle medium (Gibco) containing 10% cosmic calf serum (Gibco), 50 μg/ml penicillin-streptomycin, 2 mM L-glutamine, and 10 mM HEPES. *T. gondii* strains used in this study were derived from the PruΔ*ku80*S/Luc strain (13) maintained *in vitro* by serial passage on HFF monolayers as previously described (23). Strains used in this study were generated using strategies previously described (24) and outlined here in Fig. S1 and 2. Primers used in the generation and confirmation of strains with *CRT* (ToxoDB: TGME49_313930) deletion (Fig. S1), *CRT* complementation, and integration of dt-ATG8 (Fig. S2) are listed in Table S1 in the supplemental material.

VAC staining. Egressed tachyzoites from HFFs were filter purified and pelleted at 1,500 $\times$ *g* for 10 min. Parasites were settled on Cell-Tak (Fisher Scientific) coated slides for 30 min, fixed in 4% formaldehyde, and stained for with RbαTgCPL (1:500) and GtαRb 594 secondary (1:1,000).

In vitro conversion. Tachyzoites were converted to bradyzoite cysts *in vitro* using previously published methods (24). In brief, tachyzoites were allowed to invade HFFs overnight under standard growing conditions. Infected cells were then grown in alkaline media (RPMI 1640 without NaHCO$_3$, 50 mM HEPES, 3% fetal bovine serum, and Pen/Strep [pH 8.2]) in an incubator without CO$_2$, with media changed every day until samples were processed.

Transmission electron microscopy. For ultrastructural observations of infected cells by thin section, samples were fixed in 2.5% glutaraldehyde in 0.1 mM sodium cacodylate and processed as described previously (25). Ultrathin sections of infected cells were stained with osmium tetraoxide before examination with Philips CM120 EM (Eindhoven, Netherlands) under 80 kV.

qPCR/plaque assay for bradyzoite viability. *In vitro* bradyzoite viability was assessed by plaque assays normalized to qPCR as previously described (13). Briefly, tachyzoites were converted to bradyzoite cysts for 7 and 14 days as described above. At these time points, bradyzoites were harvested using pepsin treatment and added to HFF monolayers for 10 days, and then the plaques were counted. Genomic DNA was extracted from an aliquot of samples using the Qiagen blood and tissue kit, and SYBR

green qPCR was performed using the primer pairs listed in Table S1 and the following reaction conditions: 98°C for 2 min, followed by 45 cycles of 98°C for 5 s, 68°C for 30 s, and 72°C for 45 s.

Microscopy. All phase-contrast and fluorescence imaging was performed on a Zeiss Axiovert Observer Z1 inverted fluorescence microscope. Exposure times within a given experiment were kept constant for all samples.

GFP intensity. After 1 and 2 weeks of tachyzoite conversion, as described above, *in vitro* cysts were fixed and stained with biotinylated dolichos (primary, 1:400; Vector Laboratories) and streptavidin Alexa 350 (secondary; 1:1,000; Life Technologies). ImageJ was used to select dolichos-stained cysts and quantify the amount of GFP coverage and intensity within the cyst. The dolichos signal was used to create a mask for further analysis by autothresholding according to the method of Li and Tam (26). Analysis under these masks was redirected to the GFP channel, where particles of between 130 to 2,300 μm^2 and 0.30 to 1.00 circularity were analyzed.

tdTomato-Atg8 intensity and size. After 1 week of tachyzoite conversion as described above, *in vitro* cysts were fixed and stained with biotinylated dolichos (primary, 1:400; Vector Laboratories) and streptavidin Alexa 350 (secondary, 1:1,000; Life Technologies). ImageJ was used to select dolichos-positive cysts and quantify the total intensity of tdTomato-Atg8 and the tdTomato-Atg8 puncta size within each cyst. Dolichos-positive structures between 200 and 2,000 μm^2 with a circularity of 0.40 to 1.00 were identified using the minimum method of autothresholding. The resulting binary images were used to create masks under which Atg8 puncta were further analyzed. tdTomato-Atg8 puncta were analyzed as being between 0.2 and 1.50 μm^2 with a circularity of 0.40 to 1.00 and were identified according to the Phansalkar method of autolocal thresholding with a radius of 15 (27).

Tachyzoite plaque assay. Intracellular tachyzoites were harvested following standard procedures, counted, and added to HFF monolayers in triplicate to quadruplicate wells. Parasites were left undisturbed for 10 days, and then the plaques were counted.

Mouse seropositivity. *Toxoplasma* IgG was measured using enzyme-linked immunosorbent assay to determine infectivity. In brief, *Toxoplasma* lysate was made from freshly lysed Pru tachyzoites that were sonicated in 1 μg/ml leupeptin, 1 μg/ml E64, TPCK (tolylsulfonyl phenylalanyl chloromethyl ketone), and 10 μg/ml A-PMSF. Plates were coated with 10 ng of antigen in coating buffer (Na$_2$CO$_3$, NaHCO$_3$ [pH 9.6]) overnight and blocked in 3% gelatin/PBS-T; serum was added in a 1:25 dilution in 1% gelatin/PBS-T, followed by incubation for 1 h at room temperature. Secondary horseradish peroxidase-conjugated GtαMs (1:1,000) was added for 1 h. Substrate was added for color development, which was then stopped with H$_2$SO$_4$. The absorbance was read at 400 nm.

Tachyzoite ingestion assay. Tachyzoite digestion was determined using an ingestion assay as previously described (12). In brief, inducible mCherry Chinese hamster ovary (CHO) cells were plated and induced with 2 μg/ml of doxycycline for 5 days. Tachyzoites were harvested from HFF cells and allowed to invade induced CHO cells for 4 h. Tachyzoites were then mechanically lysed out of host cells, purified, treated with pronase and saponin, and imaged on Cell-Tak (Fisher Scientific)-coated slides. Samples were coded at the time of initial harvesting. For each biological replicate, more than 200 tachyzoites of each genotype were analyzed for host-derived mCherry accumulation within parasites.

Western blotting. Tachyzoite lysates were prepared from purified parasites with the addition of boiled 1$\times$ sample buffer, and lysate from 3 $\times$ 10^5 tachyzoites/10 μl of sample buffer was loaded onto 10% sodium dodecyl sulfate-polyacrylamide gels. Blots were probed with antibody to TgCPL (Rb; 1:300) (10) and α-tubulin (Ms; 1:1,000; Developmental Studies Hybridoma Bank, University of Iowa) for the loading control.

Puncta measurements in LHVS-treated parasites. Tachyzoites were converted to bradyzoite cysts as described above. After 7 days of conversion, parasites were treated with 1 μM LHVS or DMSO (control) every day for 3 days. The cells were then fixed and stained with biotinylated dolichos lectin (primary, 1:400; Vector Laboratories) and streptavidin Alexa 350 (secondary, 1:1,000; Life Technologies). ImageJ was used to select dolichos-stained cysts and quantify the number and size of puncta within the cyst. Images were automatically thresholded using the MaxEntropy method to create a binary image (28). Noise was reduced by opening the image with six iterations of one pixel. Masks were created by using the "analyze particle" function, with objects between 130 and 1,900 μm^2 and a circularity of 0.30 to 1.00 being called a cyst. Under these masks, dark puncta were analyzed as follows. Phase images were Gaussian blurred with a sigma of 2 and then autolocal thresholding was performed according to the Phansalkar method (27) with a radius of 5 pixels. Objects with an area of 0.20 to 6.00 μm^2 and a circularity of 0.50 to 1.00 were analyzed as dark puncta.

***In vitro* differentiation kinetics.** Tachyzoites were converted to bradyzoite cysts as described above. Parasites were fixed at 1, 2, 3, and 4 days postconversion and stained for BAG1 (RbαBAG1, 1:1,000), a late marker for bradyzoites. These parasites express GFP under the LDH2 promoter, an early marker of bradyzoites. ImageJ was used to analyze the BAG1 and GFP coverage of each vacuole. Vacuoles were manually identified using phase images by drawing a region of interest (ROI) with the freehand tool. The ROIs were then applied to other channels for analysis as follows. The GFP and Texas Red channels were autothresholded using optimal thresholding methods for each day of conversion. The nonthresholded and thresholded ROIs were measured for pixel intensity and used to determine the overall and percent intensity for GFP and Texas Red. Vacuoles with >50% coverage were designated as cysts, and the total percentage of GFP- and BAG1-positive cysts was calculated independently.

***In vivo* cyst burden.** C57BL/6J female mice (7 to 8 weeks old; Jackson Laboratories, Bar Harbor, ME) were used in this study. Mice were injected intraperitoneally (i.p.) with purified 10^5 tachyzoites of either PruS/Luc (Pru), PruΔcrt (PΔcrt), or PruΔcrt:CRT (PΔcrt:CRT) in 200 μl of 1$\times$ phosphate-buffered saline (PBS). At 4 weeks postinfection, mice were sacrificed according to university-approved protocols. Brains were

harvested and homogenized in 1 ml of ice-cold PBS via syringing through a 20-gauge needle. Mice were coded, cysts were enumerated in 90 μl of brain homogenate (9% of the brain), and the total brain cyst numbers were calculated. Cyst burden data were pooled from two independent experiments.

In vivo parasite burden kinetics. The same inoculation conditions as described for *in vivo* cyst burden was used. At 7 and 10 days postinfection, mice were sacrificed, and the brains were harvested. Brains were homogenized in ice-cold PBS to have 50 ng of homogenate/μl of PBS. gDNA was extracted from 50 μl of homogenate using a DNeasy blood and tissue kit (Qiagen). qPCR was performed in triplicate for each sample with the indicated cycling conditions (90°C for 2 min, followed by 45 cycles of 98°C for 10 s, 56°C for 20 s, and 72°C for 20 s) using SSO Advanced SYBR green Supermix (Bio-Rad), and 300 nM concentrations of the Tox9 and Tox11 primers listed in Table S1 in the supplemental material. *T. gondii* standards of specified parasite numbers (1 to 10^5 genomes/μl) were used to quantify parasite brain burden.

In vivo cyst viability. To determine the viability of *T. gondii* cysts procured from the *in vivo* cyst burden experiment, 5 and 30 brain cysts of Pru, PΔcrt, or PΔcrt:CRT were injected i.p. into C57BL/6J female mice (7 to 8 weeks old). Mice inoculated with equivalent amounts of uninfected mouse brain homogenate were used as a negative control for infection. At 3 weeks postinfection, the mice were coded and sacrificed. Sera and brains were collected as described above for the *in vivo* cyst burden. Half of each brain homogenate was added to confluent HFF cells and monitored for parasite growth for 4.5 weeks.

Flow cytometry. Parasites were fixed with 4% formaldehyde for 15 min at room temperature, washed once with PBS, and resuspended in PBS for analysis on a LSR Fortessa flow cytometer (BD Biosciences, San Jose, CA) using BD FACSDiVa software (BD Biosciences). Data were analyzed with FlowJo (BD Biosciences) using the following gating: fluorescein isothiocyanate-positive parasites were characterized as bradyzoites; the amount of tdTomato-ATG8 in bradyzoites was then determined by using the 561-nm signal. All experimental samples for flow analysis were coded.

Statistics. Data were analyzed using GraphPad prism. For each data set, outliers were identified and removed using ROUT with a Q value of 0.1%. Data were then tested for normality and equal variance. If the data passed, one-way analysis of variance (ANOVA) and Tukey's multiple-comparison analyses were performed. If the data failed, a Mann-Whitney U test or Kruskal-Wallis test with Dunn's multiple comparison was performed.

SUPPLEMENTAL MATERIAL

Supplemental material for this article may be found at https://doi.org/10.1128/mBio .01324-19.

FIG S1, TIF file, 0.6 MB.
FIG S2, TIF file, 2.2 MB.
FIG S3, TIF file, 0.3 MB.
FIG S4, TIF file, 0.2 MB.
FIG S5, TIF file, 0.1 MB.
TABLE S1, DOCX file, 0.1 MB.

ACKNOWLEDGMENTS

REFERENCES

1. Commodaro AG, Belfort RN, Rizzo LV, Muccioli C, Silveira C, Burnier MN, Jr, Belfort R, Jr. 2009. Ocular toxoplasmosis: an update and review of the literature. Mem Inst Oswaldo Cruz 104:345–350. https://doi.org/10.1590/s0074-02762009000200030.

2. Khan K, Khan W. 2018. Congenital toxoplasmosis: an overview of the neurological and ocular manifestations. Parasitol Int 67:715–721. https://doi.org/10.1016/j.parint.2018.07.004.

3. Ozgonul C, Besirli CG. 2017. Recent developments in the diagnosis and treatment of ocular toxoplasmosis. Ophthalmic Res 57:1–12. https://doi.org/10.1159/000449169.

4. Winstanley P. 1995. Drug treatment of toxoplasmic encephalitis in acquired immunodeficiency syndrome. Postgrad Med J 71:404–408. https://doi.org/10.1136/pgmj.71.837.404.

5. Torrey EF, Bartko JJ, Lun ZR, Yolken RH. 2007. Antibodies to *Toxoplasma gondii* in patients with schizophrenia: a meta-analysis. Schizophr Bull 33:729–736. https://doi.org/10.1093/schbul/sbl050.

6. Okusaga O, Langenberg P, Sleemi A, Vaswani D, Giegling I, Hartmann AM, Konte B, Friedl M, Groer MW, Yolken RH, Rujescu D, Postolache TT. 2011. *Toxoplasma gondii* antibody titers and history of suicide attempts in patients with schizophrenia. Schizophr Res 133:150–155. https://doi.org/10.1016/j.schres.2011.08.006.

7. Xiao J, Prandovszky E, Kannan G, Pletnikov MV, Dickerson F, Severance EG, Yolken RH. 2018. *Toxoplasma gondii*: biological parameters of the connection to schizophrenia. Schizophr Bull 44:983–992. https://doi.org/10.1093/schbul/sby082.

8. Tyebji S, Seizova S, Hannan AJ, Tonkin CJ. 2019. Toxoplasmosis: a pathway to neuropsychiatric disorders. Neurosci Biobehav Rev 96:72–92. https://doi.org/10.1016/j.neubiorev.2018.11.012.

9. Montoya JG, Liesenfeld O. 2004. Toxoplasmosis. Lancet 363:1965–1976. https://doi.org/10.1016/S0140-6736(04)16412-X.

10. Parussini F, Coppens I, Shah PP, Diamond SL, Carruthers VB. 2010. Cathepsin L occupies a vacuolar compartment and is a protein maturase within the endo/exocytic system of *Toxoplasma gondii*. Mol Microbiol 76:1340–1357. https://doi.org/10.1111/j.1365-2958.2010.07181.x.

11. Dou Z, McGovern OL, Di Cristina M, Carruthers VB. 2014. *Toxoplasma gondii* ingests and digests host cytosolic proteins. mBio 5:e01188. https://doi.org/10.1128/mBio.01188-14.

12. McGovern OL, Rivera-Cuevas Y, Kannan G, Narwold AJ, Jr, Carruthers VB. 2018. Intersection of endocytic and exocytic systems in *Toxoplasma gondii*. Traffic 19:336–353. https://doi.org/10.1111/tra.12556.

13. Di Cristina M, Dou Z, Lunghi M, Kannan G, Huynh MH, McGovern OL, Schultz TL, Schultz AJ, Miller AJ, Hayes BM, van der Linden W, Emiliani C, Bogyo M, Besteiro S, Coppens I, Carruthers VB. 2017. Toxoplasma depends on lysosomal consumption of autophagosomes for persistent infection. Nat Microbiol 2:17096. https://doi.org/10.1038/nmicrobiol.2017.96.

14. Larson ET, Parussini F, Huynh MH, Giebel JD, Kelley AM, Zhang L, Bogyo M, Merritt EA, Carruthers VB. 2009. *Toxoplasma gondii* cathepsin L is the primary target of the invasion-inhibitory compound morpholinurea-leucyl-homophenyl-vinyl sulfone phenyl. J Biol Chem 284:26839–26850. https://doi.org/10.1074/jbc.M109.003780.

15. Warring SD, Dou Z, Carruthers VB, McFadden GI, van Dooren GG. 2014. Characterization of the chloroquine resistance transporter homologue in *Toxoplasma gondii*. Eukaryot Cell 13:1360–1370. https://doi.org/10.1128/EC.00027-14.

16. Maughan SC, Pasternak M, Cairns N, Kiddle G, Brach T, Jarvis R, Haas F, Nieuwland J, Lim B, Muller C, Salcedo-Sora E, Kruse C, Orsel M, Hell R, Miller AJ, Bray P, Foyer CH, Murray JA, Meyer AJ, Cobbett CS. 2010. Plant homologs of the *Plasmodium falciparum* chloroquine-resistance transporter, PfCRT, are required for glutathione homeostasis and stress responses. Proc Natl Acad Sci U S A 107:2331–2336. https://doi.org/10.1073/pnas.0913689107.

17. Juge N, Moriyama S, Miyaji T, Kawakami M, Iwai H, Fukui T, Nelson N, Omote H, Moriyama Y. 2015. *Plasmodium falciparum* chloroquine resistance transporter is a H$^+$-coupled polyspecific nutrient and drug exporter. Proc Natl Acad Sci U S A 112:3356–3361. https://doi.org/10.1073/pnas.1417102112.

18. Thornton LB, Teehan P, Floyd K, Cochrane C, Bergmann A, Riegel B, Stasic AJ, Di Cristina M, Moreno SNJ, Roepe PD, Dou Z. 2019. An ortholog of *Plasmodium falciparum* chloroquine resistance transporter (PfCRT) plays a key role in maintaining the integrity of the endolysosomal system in *Toxoplasma gondii* to facilitate host invasion. PLoS Pathog 15:e1007775. https://doi.org/10.1371/journal.ppat.1007775.

19. Fox BA, Falla A, Rommereim LM, Tomita T, Gigley JP, Mercier C, Cesbron-Delauw MF, Weiss LM, Bzik DJ. 2011. Type II *Toxoplasma gondii* KU80 knockout strains enable functional analysis of genes required for cyst development and latent infection. Eukaryot Cell 10:1193–1206. https://doi.org/10.1128/EC.00297-10.

20. Rosenthal PJ, McKerrow JH, Aikawa M, Nagasawa H, Leech JH. 1988. A malarial cysteine proteinase is necessary for hemoglobin degradation by *Plasmodium falciparum*. J Clin Invest 82:1560–1566. https://doi.org/10.1172/JCI113766.

21. Pulcini S, Staines HM, Lee AH, Shafik SH, Bouyer G, Moore CM, Daley DA, Hoke MJ, Altenhofen LM, Painter HJ, Mu J, Ferguson DJ, Llinas M, Martin RE, Fidock DA, Cooper RA, Krishna S. 2015. Mutations in the *Plasmodium falciparum* chloroquine resistance transporter, PfCRT, enlarge the parasite's food vacuole and alter drug sensitivities. Sci Rep 5:14552. https://doi.org/10.1038/srep14552.

22. Miranda K, Pace DA, Cintron R, Rodrigues JC, Fang J, Smith A, Rohloff P, Coelho E, de Haas F, de Souza W, Coppens I, Sibley LD, Moreno SN. 2010. Characterization of a novel organelle in *Toxoplasma gondii* with similar composition and function to the plant vacuole. Mol Microbiol 76:1358–1375. https://doi.org/10.1111/j.1365-2958.2010.07165.x.

23. Di Cristina M, Ghouze F, Kocken CH, Naitza S, Cellini P, Soldati D, Thomas AW, Crisanti A. 1999. Transformed *Toxoplasma gondii* tachyzoites expressing the circumsporozoite protein of *Plasmodium knowlesi* elicit a specific immune response in rhesus monkeys. Infect Immun 67:1677–1682.

24. Lunghi M, Galizi R, Magini A, Carruthers VB, Di Cristina M. 2015. Expression of the glycolytic enzymes enolase and lactate dehydrogenase during the early phase of *Toxoplasma* differentiation is regulated by an intron retention mechanism. Mol Microbiol 96:1159–1175. https://doi.org/10.1111/mmi.12999.

25. Coppens I, Joiner KA. 2003. Host but not parasite cholesterol controls *Toxoplasma* cell entry by modulating organelle discharge. Mol Biol Cell 14:3804–3820. https://doi.org/10.1091/mbc.e02-12-0830.

26. Li CH, Tam P. 1998. An iterative algorithm for minimum cross entropy thresholding. Pattern Recognition Lett 19:771–776. https://doi.org/10.1016/S0167-8655(98)00057-9.

27. Phansalkar N, More S, Sabale A, Joshi MS. 2011. Adaptive local thresholding for detection of nuclei in diversity stained cytology images. International Conference on Communications and Signal Processing, Institute for Electrical and Electronics Engineers, Piscataway, NJ, USA.

28. Kapur JN, Sahoo PK, Wong A. 1985. A new method for gray-level picture thresholding using the entropy of the histogram. Computer Vision Graphics Image Processing 29:273–285. https://doi.org/10.1016/0734-189X(85)90125-2.